Author's Manuscript - Public Access

Sequence-Optimized Peptide Nanofibers as Growth Stimulators for Regeneration of Peripheral Neurons

Corinna Schilling, Thomas Mack, Selene Lickfett, Stefanie Sieste, Francesco S. Ruggeri, Tomas Sneideris, Arghya Dutta, Tristan Bereau, Ramin Naraghi, Daniela Sinske, Tuomas P. J. Knowles, Christopher V. Synatschke, Tanja Weil,* and Bernd Knöll*

Sequence-Optimized Peptide Nanofibers as Growth Stimulators for Regeneration of Peripheral Neurons

Corinna Schilling[1,#], Thomas Mack[2, #,] Selene Lickfett[1], Stefanie Sieste[2], Francesco S. Ruggeri[3], Tomas Sneideris[3], Arghya Dutta[4], Tristan Bereau[4], Ramin Naraghi[5], Daniela Sinske[1], Tuomas P. J. Knowles[3], Christopher V. Synatschke[6], Tanja Weil[2, 6,*], Bernd Knöll[1,*]

[1] Institute of Physiological Chemistry
Ulm University
Albert-Einstein-Allee 11
89081 Ulm
Germany

[2] Institute of Inorganic Chemistry I
Ulm University
Albert-Einstein-Allee 11
89081 Ulm
Germany

[3] Department of Chemistry
University of Cambridge
Cambridge CB2 1EW
UK

[4] Max Planck Institute for Polymer Research
Ackermannweg 10
55128 Mainz
Germany

[5] Department of Neurosurgery
German Armed Forces Hospital Ulm
Oberer Eselsberg 40
89081 Ulm
Germany

[6] Department Synthesis of Macromolecules
Max Planck Institute for Polymer Research
Ackermannweg 10
55128 Mainz
Germany

*corresponding authors:
Bernd Knöll: phone +49 731 50033839, bernd.knoell@uni-ulm.de
Tanja Weil: phone +49 6131 379131,   weil@mpip-mainz.mpg.de

Abstract

There is an urgent need for biomaterials that support tissue healing, particularly neuronal regeneration. We identified in a medium throughput screen novel self-assembling peptide (SAP) sequences that form fibrils and stimulated nerve fiber growth of peripheral nervous system (PNS) derived neurons. Based on the peptide sequences and fibril morphologies and by applying rational data-mining, important structural parameters were elucidated that were essential for high neuronal activity. Three SAPs (SAP[1e], SAP[2e] and SAP[5c]) significantly enhanced adhesion and growth of DRG (dorsal root ganglion) neurons. These SAPs formed two and three-dimensional matrices that served as bioactive scaffolds stimulating cell adhesion and growth. The newly discovered SAPs also supported the growth of CNS neurons and glia cells. Subsequently, we analyzed the potential of SAPs to enhance PNS regeneration *in vivo*. The facial nerve driving whisker movement in mice was unilaterally injured. Notably, SAPs persisted for up to three weeks in the nerve injury site indicating highly adhesive properties and stability. After SAP administration, more motorneurons incorporating markers for successive regeneration were observed. Recovery of whisker movement was elevated in SAP-injected mice. In summary, we identified a novel set of short peptide sequences that formed fibrils and efficiently enhanced adhesion, growth and regeneration of neurons *in vivo* without the necessity to attach or release hormones or growth factors. We also correlated sequences and structural information with neuronal growth, which provided essential features of bioactive PNFs and paves the way to rationally designed biomaterials.

1 Introduction

Tissue damage results in cavity formation thereby disrupting cell-cell interactions. Several strategies in tissue engineering aim at filling these lesions with biomaterials facilitating cellular re-connection and functional recovery [1]. In the peripheral nervous system (PNS) injuries split the nerves into two nerve stumps separated by a gap ranging between millimeters to centimeters. The current therapeutic gold standard is surgical end-to-end suturing of disconnected nerves [2]. However, for larger gaps, nerve interponates so-called autografts from the same patient bridge the gap between both stumps [3]. The intrinsic regenerative potential of transected PNS nerves is superior to injured central nervous system (CNS) axons [4]. Still, also in the PNS complete axon regeneration and full functional recovery often cannot be achieved. One drawback in using autologous nerves and blood vessels as donor tissues is the fact that this approach requires further surgery and may induce ectopic pain sensation [1]. These limitations have encouraged new biomaterial-based therapeutic strategies to bridge disconnected nerve stumps and enhance nerve reconnection and functional recovery in a non-invasive fashion [1b].

Self-assembling peptides (SAPs) have emerged as a promising biomaterial in regenerative medicine [1a, 5]. These peptides undergo spontaneous self-assembly and depending on the peptide sequence, various nanostructures such as fibers, rods and tubes have been formed [5b]. Peptide nanofibers (PNFs) can form networks resembling the extracellular matrix in key aspects that could serve as an artificial scaffold structure promoting cell adhesion and growth [6]. Certain PNFs revealed high biocompatibility and did not promote tissue inflammation [1a]. Further functionalities have been attached either to the peptide sequences before assembly or to the already formed fibers, including epitopes of extracellular matrix proteins such as laminin or fibronectin [7], polydopamine [8], glycosaminoglycans [9] or growth factors [10] including BDNF [11].

3

These biomimetic SAPs increased focal adhesion assembly, which is attractive for processes such as axonal regeneration [12]. In addition, enhanced nerve fiber growth from primary rodent neurons has been demonstrated on SAP matrices [8, 13]. In these cell culture experiments, SAPs enhanced axon re-growth and regeneration. So far, SAPs have mainly been used in CNS injury models such as spinal cord lesions. These SAPs reduced glial scarring and neuroinflammation while simultaneously promoting outgrowth and functional recovery of severed axons [7b, 7c, 14]. In contrast, there are only few studies of PNFs in PNS regeneration. So far, two model systems of PNS regeneration, i.e. facial [15] or sciatic nerve regeneration [16] were mainly employed. For those studies, different PNFs were used including nanofibers composed of C16VVVAAAEEE [15] or RADA 16-I derived SAPs with two functional motifs IKVAV and RGD [16a, 16b]. These nanofibers were incorporated into collagen tubes [15], poly lactic-co-glycolic acid (PLGA) tubes [16b, 16c] or hydrogels [16a]. To the best of our knowledge, "free" nanofibers without any filling into conduits have not been applied yet. The preparation of such conduits is labor- and cost-intensive and it would be advantageous to instead simply inject biomaterials such as PNFs into the injury site.

A direct comparison of the results in these studies is difficult for several reasons: The reported animal studies used different parameters to assess functional regeneration such as histology, gene expression and functional tests. For instance, nanofiber-filled neurografts were comparable to the gold-standard (i.e. a nerve autograft) in enhancing nerve action potential propagation after facial nerve injury [15]. In a different histological parameter, the nanofiber-filled neurograft was even superior to the autograft and restored the axon diameter of injured axons almost completely to pre-injury levels [15]. However, most available studies could only demonstrate a limited increase in individual regeneration parameters, which did not exceed effects observed with nerve autografts.

Herein, we have identified short SAPs that formed PNFs capable of enhancing PNS regeneration without additional bioactive peptides, growth factors, or hormones. Also, no filling into conduits was required. Bioactive SAPs were identified by screening a peptide library consisting of short peptide sequences with an average of nine amino acids per peptide that were stabilized by intermolecular β-sheet structures. We used the facial nerve in mice to study PNS regeneration. Facial motorneurons (MN) in the brain are connected by the facial nerve with several facial muscles to control e.g. whisker movement. This injury model has the advantage that regeneration success can be monitored by histological means (e.g. retrograde transport of fluorescent racer along axons) and also on the functional level. For the latter, recovery of whisker movement after injury is quantified by videotaping with a high-speed camera.

In other studies on nerve regeneration, SAPs were introduced into hydrogels or tubes, which can lead to heterogeneous distribution and aggregation of the material [15-16]. We have directly injected dispersed SAP nanofibers in solution at the lesion site, where the SAPs revealed highly adhesive behavior and persisted at the lesion site for several weeks. The SAPs identified from our library enhanced axon regeneration and they augmented adhesion and growth of primary PNS neurons. The most bioactive SAP[5c] was tested *in vivo* in a mouse model resulting in enhanced facial nerve regeneration as well as functional recovery of whisker movement.

To the best of our knowledge, this is the first study on the identification of SAPs based on the correlation of structural parameters and bioactivity yielding bioactive fibrils that supported neuronal growth and nerve regeneration without the necessity of additional components such as growth factors, extracellular matrix domains or hormones. We believe that the newly discovered SAPs form a bioactive and convenient to use nanomaterial with high potential for regenerative medicine.

2 Results

2.1 Design and synthesis of the SAP fibril library

A peptide library was prepared consisting of about 27 different peptide sequences *via* Fmoc solid phase peptide synthesis (Table 1, Table S1). The sequences were designed based on the peptide sequence QCKIKQIINMWQ originating from the glycoprotein $GP120_{417-428}$ of Human Immunodeficiency Virus (HIV) that enhanced the cellular uptake of virions [17]. Most of the sequences comprised the amphiphilic six amino acid sequences KIKIQI or KFKFQF (Table 1). Almost all SAPs had an overall positive net charge thus being more likely to interact with negatively charged cell membranes. In accordance, the negatively charged SAP^{8a} (Table 1) failed to enhance cell adhesion and growth (Figure S1). In some cases, functionalities such as an Fmoc protection group (SAP^{1e}) or the RGD sequence (SAP^{5a} to SAP^{6b}) were added at the N- or C-terminus to further enhance self-assembly and possibly cell adhesion (Table1) [18]. The peptides listed in Table 1 were purified with high performance liquid chromatography (HPLC) and characterized by mass spectrometry and the corresponding spectra are given in Table S1 and Figure S2.

To induce fibril formation, SAPs were dissolved in DMSO at 10 mg/mL as a non-selective solvent, followed by 10-fold dilution in PBS (phosphate buffered saline or double-distilled water, ddH_2O, for SAP^{1e}) to induce self-assembly (Figure 1A). The conversion rate of the SAPs to PNFs was determined using an assay developed in our group [21]. Here, the conversion rate measures the amount of peptide monomers that form fibers in solution. High conversion rates were indicated by 70-100% (e.g. SAP^{2e}, SAP^{5c}) whereas moderate and low fibril formation was obtained for SAP^{5d} and SAP^{1d}, respectively (Table 1). Transmission electron microscopy (TEM) was used to acquire 2-D micrographs and analyze the SAP aggregation state. High aspect ratio PNFs were found for most SAPs (Figure 1B, Figure S3) with a variety of morphologies like sheet-

like aggregates (SAP[4e]), twisted fibrils (SAP[1b]) or amyloid-like fibrils (SAP[2e]; Figure 1B,

Figure S3). A summary of the observed morphologies ("+" = fibers, "0" = aggregates,

"-" = no assembly) is given in Table 1.

Table 1
Characteristics of the SAP library.
SAP #, SAP name and 1 letter code of amino acid sequence. Qualitative fibril formation determined via transmission electron microscopy ("+" for fibrils, "0" for aggregates and "-" for no fibrils'/aggregates). PNF form. refers to PNF formation. Zetapotential calculated by electrophoretic mobility. FT-IR band in amide I range. Conversion rate ("conver. rate") as the amount of SAPs forming PNFs. Ability to bind Proteostat ("PROT bind.", "+" for ≥ 10 n-fold fluorescence enhancement and "-" for ≤ 10 n-fold fluorescence enhancement).

#	SAP name	sequence	PNF form.	Zetapotential (mV)	FT-IR (cm^{-1})	conver. rate (%)	PROT bind.
1	SAP[1a]	KIKIKIQI	-	10.5 ± 0.8	1626	80	+
2	SAP[1b]	KLKLKLQL	+	-0.8 ± 1.3	1626	n.d.	-
3	SAP[1c]	KIKIQIII	+	19.5 ± 2.9	1629	87	+
4	SAP[1d]	KIKIQI	-	n.d.	1630	5.2	-
5	SAP[1e] (H_2O)	Fmoc-KIKIQI	+	54.7 ± 2.1	1628	94	+
	SAP[1e] (PBS)	Fmoc-KIKIQI	+	3.0 ± 6.6	1628	31	+
6	SAP[2a]	KFKFQFFF	+	19.3 ± 0.6	1635	99	+
7	SAP[2b]	KFKFQF	-	n.d.	1626	83	-
8	SAP[2c]	KFKFKFQF	0	22.5 ± 0.8	1630	94	+
9	SAP[2d]	KFKFQFNM	+	20.2 ± 1.9	1628	94	-
10	SAP[2e]	CKFKFQF	+	22.3 ± 1.4	1627	95	+
11	SAP[3a]	KIKIQINMWQ	+	11.4 ± 5.9	1629	93	+
12	SAP[3b]	CKIKIQINMWQ	+	10.7 ± 2.8	1632	87	+
13	SAP[3c]	KIKIQINM	+	41.9 ± 1.1	1627	64	+
14	SAP[4a]	CKIKQIINM	+	11.5 ± 6.6	1630	45	+
15	SAP[4b]	CKIKIQIII	+	19.0 ± 0.3	1630	n.d.	+
16	SAP[4c]	CKIKIQINM	+	22.3 ± 0.6	1628	72	+
17	SAP[4d]	CKIKQII	+	n.d.	1635	55	-
18	SAP[4e]	CKIKIQI	+	17.4 ± 1.1	1626	54	+
19	SAP[4f]	CKIKQIINMWQ	+	9.7 ± 2.0	1631	n.d.	+
20	SAP[5a]	RGDKIKIQINMC	+	9.1 ± 2.2	1627	60	+
21	SAP[5b]	RGDKIKIQINM	+	24.0 ± 0.5	1627	48	+
22	SAP[5c]	RGDKIKIQIC	+	21.7 ± 1.2	1627	80	+
23	SAP[5d]	RGDKIKIQINMWQ	+	8.7 ± 2.3	1627	66	+
24	SAP[6a]	KIKIQIRGD	+	-10.1 ± 1.3	1626	n.d.	+
25	SAP[6b]	CKIKIQIRGD	0	3.1 ± 0.1	1627	91	-
26	SAP[7a]	HHHHKIKIKIKIWWWW	0	18.1 ± 0.5	1628	96	+
27	SAP[7b]	KIKIKIWW	0	21.0 ± 0-3	1627	92	-
28	SAP[8a]	EIEIQINM	+	-36.0 ± 3.5	1630	77	+

2.2 Identification of nerve fiber growth stimulating SAPs by automated screening

All PNFs were then investigated regarding their potential to promote cell adhesion and growth. The SAPs were coated as two-dimensional matrix on glass coverslips to assess their ability to interact with PNS neurons. Adult mouse dorsal root ganglion (DRG) neurons were used as well-established PNS neuron cell type [23]. In culture, neuronal cell bodies form several protrusions, so-called neurites that differentiate into either an axon or a dendrite. Interestingly, we observed that neurite tips, so-called growth cones, were frequently contacting SAP positive areas on the coverslip (Figure 1C). The spatial pattern of SAP localization on glass surfaces was further analyzed by scanning electron microscopy (Figure 1D-F). Typically, PNFs were arranged in networks (Figure 1F, G) forming plaques with areas up to 1 mm^2 (Figure 1D). Neurons localized on top of these plaques (Figure 1D) contacted the PNFs with several protrusions (arrows in Figure 1E, F).
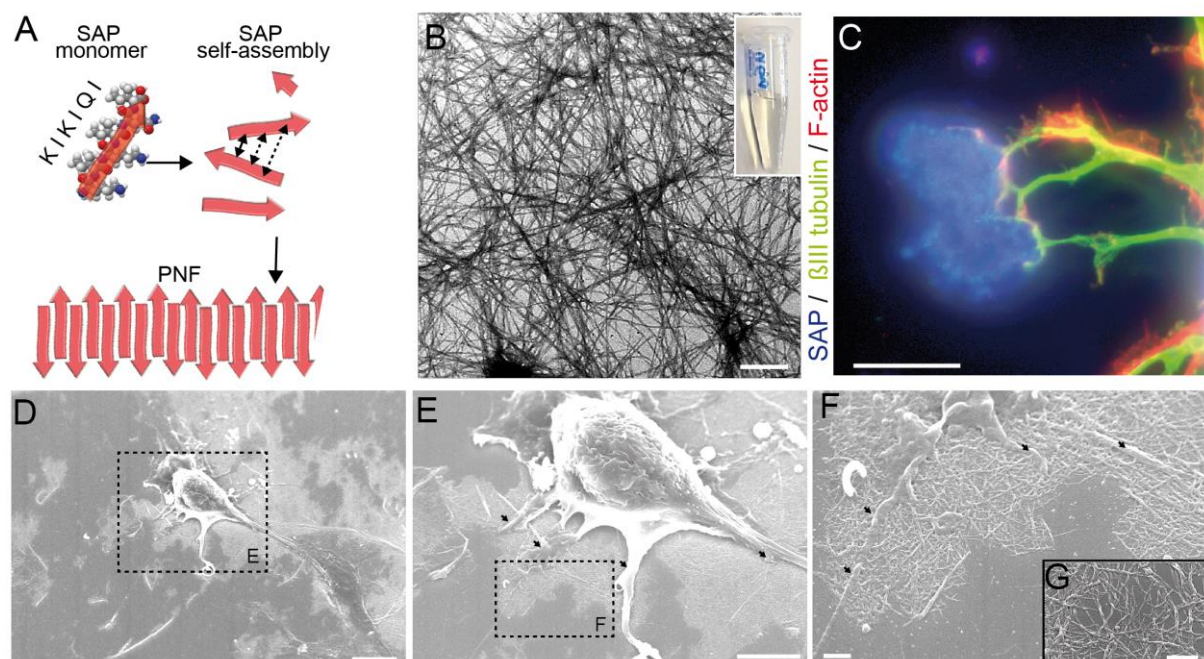

Figure 1. SAPs form PNFs that arrange in networks that can serve as scaffold for neuronal cell adhesion. (A) Schematic illustration of SAP assembly forming PNFs. A SAP monomer consisting of the amino acid sequence KIKIQI interacts with other monomers to form PNFs. (B) TEM picture of PNFs based on SAP[1e] in solution. PNF are up to several 100 μm in length. (C) PNFs form plaques (blue) on glass coverslips serving as adhesion points for nerve fibers (green). (D-G) Scanning EM pictures of primary neurons plated on SAP[1e] PNFs. Neurons contact PNFs with several cellular protrusions (arrows in E, F) and PNFs are arranged in networks (F, G).

In the next step, 27 different SAPs were screened for their ability to enhance adhesion and neurite growth using an automated Olympus ScanR microscope (Figure 2; Figure S4). For this, glass dishes were coated with 25 μg/mL SAP solutions. As negative control, glass surfaces remained uncoated. The SAP activity on neurite growth was compared to a laminin-derived peptide (Cys-lam) used as an established positive control (Figure 2B; [24]). Cys-laminin also forms nanofibers and was added on top of poly-l-lysine (PLL) pre-coated glass (PLL/Cys-lam). DRG neurons were cultured in nerve growth factor (NGF) supplemented medium for 24 h.

In order to measure the activity of SAPs on neurons, we quantified three parameters (Figure 2 and Figure S4). i) The number of attaching neurons was calculated by counting the number of DAPI and βIII tubulin double positive cells. ii) The neuronal area (revealed by the sum of all βIII tubulin signals/neuron) was automatically measured (see materials & methods). Here, each neuron was grouped into three categories according to the total βIII tubulin area determined (large, medium and small neurons; see materials & methods). Neurons with the largest area are typically also those neurons with longest neurites. To directly estimate neurite length, we assessed the length of the longest neurite/neuron with Axiovision software (Figure S4B). iii) The number of branches per neuron was quantified with a Sholl analysis (Figure S4). SAPs with highest biological activity should also enhance the number of attaching neurons, induce a high number of branches and elevate the neuronal area strongest, thereby elevating the percentage of neurons classifying for "large neurons" in comparison to less active SAPs.

DRG neurons cultured on uncoated glass (Figure 2A, E) were not able to adhere or protrude neurites whereas PLL/Cys-lam (Figure 2B, F) coating enhanced both parameters. Inspection of the SAP library revealed that many but not all SAPs improved adhesion of non-neuronal and neuronal cells and promoted nerve fiber

growth (Figure 2I; Figure S4). The number of neurons grown on SAP^{5c} or SAP^{2e} was almost identical to our positive control PLL/Cys-lam (Figure S4). In addition, coating with SAP^{5c} or SAP^{2e} had a strong impact on neurite growth since many neurons were grouped into "medium" or "large" neurons (Figure 2I) and they also enhanced the number of branches/neuron (Figure S4C). Both, SAP^{5c} or SAP^{2e} revealed a much stronger activity on neurite growth than the negative control glass and many other SAPs and they reached approximately 50-60% of the values obtained for the PLL/Cys-lam positive control (Figure 2I).
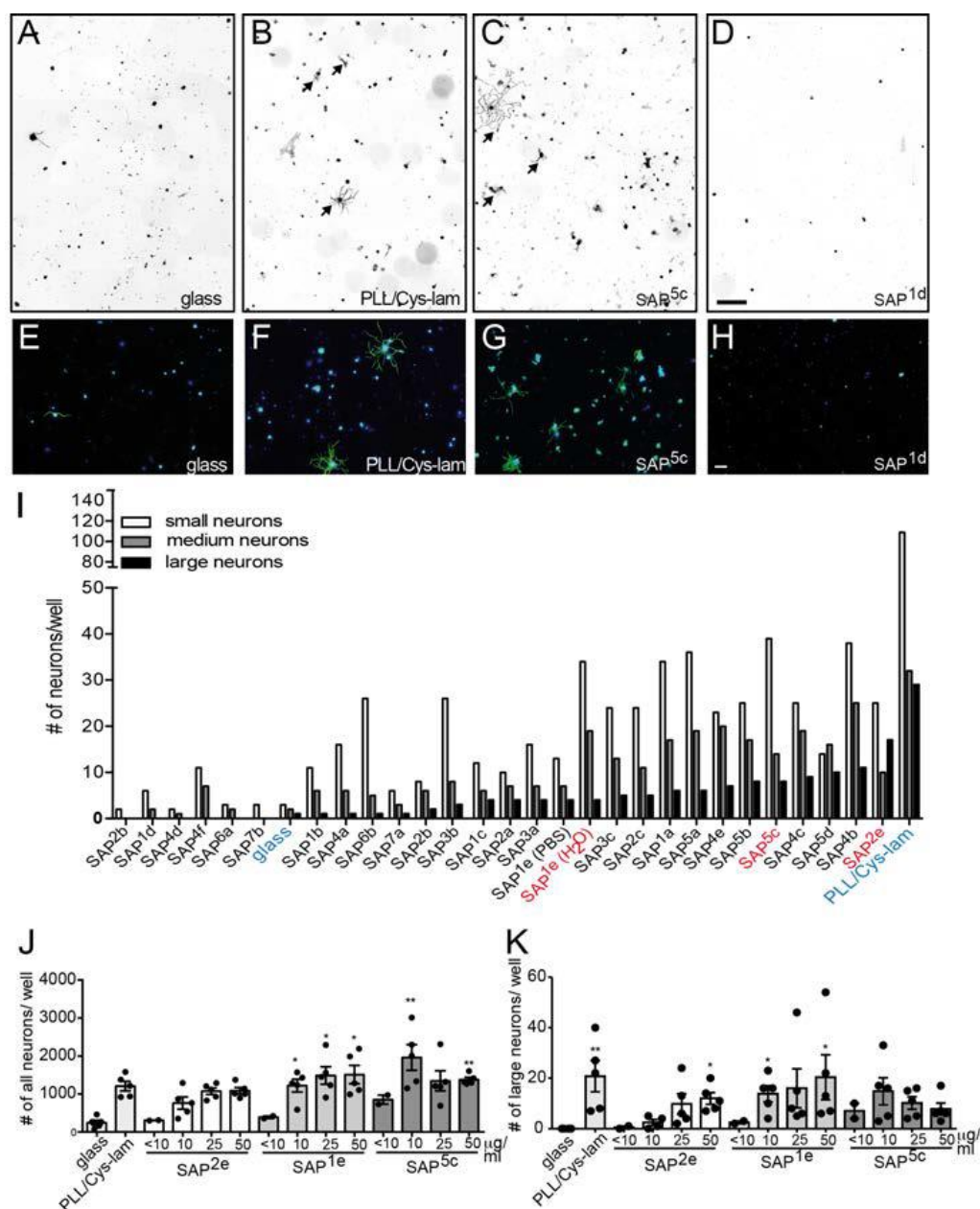
Figure 2. SAPs stimulate adhesion and outgrowth of PNS neurons
(A-H) DRG neurons were plated on coverslips without coating (A, E), or coated with PLL/Cys-lam (B, F), SAP[5c] (C, G) or SAP[1d] (D, H). After 24 h in culture, neurons were stained with βIII tubulin (black in A-D; green in E-H) and DAPI to label cell nuclei (E-H). (E-H) show higher magnifications of individual neurons. SAP[5c] stimulated neuronal adhesion and growth (C, G), in opposite to SAP[1d] (D, H). (I) Quantification by grouping neurons according to their total area into small, medium and large neurons. All SAPs were ranked with regard to the number of large neurons. The positive control PLL/Cys-lam was placed top, whereas the negative control glass was positioned at the bottom. Several SAPs, including SAP[1e], SAP[5c] and SAP[2e] (in red), used for further analysis, stimulated cell adhesion and growth almost to the same extent as PLL/Cys-lam. (J, K) Different concentrations of SAP[2e], SAP[1e] and SAP[5c] were used to coat coverslips. Below 10 µg/ml, SAPs did not promote neuronal adhesion (J) and growth (K). Above 10 µg/ml SAPs stimulated both parameters with no effect by further enhancing SAP concentration except for SAP[2e]. For "<10 µg/ml" data from 1 and 5 µg/ml were pooled. Each circle represents one culture derived from one mouse. Statistical significance was calculated in relation to glass. Scale-bars (A-D) = 500 µm; (E-H) = 100 µm.

Interestingly, attachment of an Fmoc-protection group in SAP[1e] enhanced neuronal growth (Figure 2I; Figure S4) compared to the unprotected backbone (SAP[1d]), a finding in agreement with a previous report using different Fmoc-protected SAPs [25]. We noted that RGD functionalization at the SAP N-terminus (e.g. SAP[5b], SAP[5c], SAP[5d]) also showed a positive effect and further enhanced SAP activity compared to the backbone alone. Interestingly, however, a C-terminal RGD (e.g. SAP[6a]) revealed the opposite effect and reduced neuron outgrowth (Figure 2I; Figure S4).

SAP[5c], SAP[1e] and SAP[2e] showed the most promising activity as revealed by three parameters i) the impact of the SAP in enhancing numbers of neurons adhering to the SAP coated coverslip (Figure S4A), ii) the number of branches (Figure S4C) and iii) the potential to elevate the neuronal area (Figure 2I) and average length of the longest neurite (Figure S4B) as an indication for their potential to stimulate neuronal growth (Figure 2I). Thus, these three SAPs were selected for a more in-depth investigation in additional independent experiments (Figure 2J, K). The three selected SAPs were analyzed for a concentration-dependent effect (Figure 2J, K). We found that for all cases, concentrations of about 10 µg/mL were sufficient to induce bioactivity. Notably, only SAP[2e] showed a strong concentration-dependent increase in activity on neuronal

adhesion (Figure 2J) and outgrowth (Figure 2K), whereas SAP[1e] and SAP[5c] activity could not be further augmented above a concentration of 10 μg/mL.

So far, all SAPs were tested in the presence of NGF. Notably, when omitting NGF, SAP[1e] and SAP[5c] were as efficient or even better in stimulating neurite growth compared to PLL/Cys-lam (Figure S4). Finally, we assessed whether SAPs also promoted CNS neuron growth (Figure S5). For this, mouse primary cerebellar neurons were plated on SAPs. Indeed, as observed for PNS neurons (Figure 2), some SAPs also enhanced outgrowth of CNS neurons as well (Figure S5). The *in vitro* screen of our original SAP library allowed the identification of novel SAPs that formed PNFs with high conversions that stimulated cell growth and adhesion in general and in particular of primary mouse PNS and CNS neurons.

2.3. Correlation of SAP sequences and PNF morphologies with neuronal activity

To gain insights into the various structural features of the identified SAPs that could be responsible for high neuron outgrowth, structure-property relationships analysis was accomplished. First, we related the SAP amino acid sequences to their neuronal activity in a data mining approach (Figure 3A).[26] Then, the resulting PNFs were studied to assess their physicochemical properties such as PNF morphology, surface charge, β-sheet content, persistence length, and stiffness and correlate these parameters to their neuronal activity.

The data mining approach was accomplished based on the identification of recurring patterns of amino acid sequences that are present in high-activity SAPs and, simultaneously, are absent in low or medium active SAPs. However, this search was challenging for the following reasons. Firstly, it is not feasible to experimentally test the activity of all possible sequence combinations, or even a sizable subset thereof, which relates mainly to the problem of dimensionality. Secondly, already minor changes to

an SAP sequence can lead to a major change in their activity. For example, by extending the sequence of SAP[2b] (KFKFQF) with a single cysteine residue (SAP[2e], CKFKFQF), the neuronal activity was significantly enhanced (Figure 2).

To render this high-dimensional problem tractable, we simplified the system by coarse-graining the amino acids into four basic features according to their hydrophobicity and charge, namely hydrophobic (H^0), hydrophilic (P^0), positively charged (P^+), and negatively charged (P^-) (Table S2). This simplification drastically reduced the number of possible sequences, while keeping the essential chemical features intact. With these coarse-grained SAP features, we then built a library of amino acid patterns. We composed sequence units of length 3 to 5 considering all possible combinations of the four features at each sequence position. Further repetitions of these units provided us with a comprehensive library of polypeptide patterns (1344 in total, see Figure S6 and supporting text). These patterns were subsequently compared to the SAPs using an overlap index 'I' (supplementary Eq. 2). We then ranked patterns by means of a score (supplementary Eq. 3) that favors features present in high-activity SAPs and penalizes those found in the low- and medium-activity sequences. Polypeptide patterns with high scores represent potential candidates for high neuronal activity. In a final step, these high score candidates were further analyzed for the variability of the amino acid features along the peptide sequence (Figure S7). We found that some features, particularly those at positions 1, 2, 4, and 5, were highly conserved in the patterns predicted for high neuronal activity, while the feature at position 3 has a higher variability. The most likely pattern to yield high activity SAPs was identified as the sequence $H^0P^+H^0P^+H^0$, shown in Figure 3, with alternating hydrophobic and positively charged amino acids along the peptide chain. The predicted pattern is robust as it consistently occurred in an out-of-sample analysis (Figure S8 and supporting text). In addition, we compared the predicted pattern to peptide sequences with high neuronal

activity that were reported in the literature (Table S3, Figure S9). We observed a broad range of overlap values. However, other SAPs belonging to the amphiphilic peptide or RADA family only showed moderate to low overlap. This result is conceivable as these SAPs belong to very different regions of the sequence space and they have quite different structural properties.
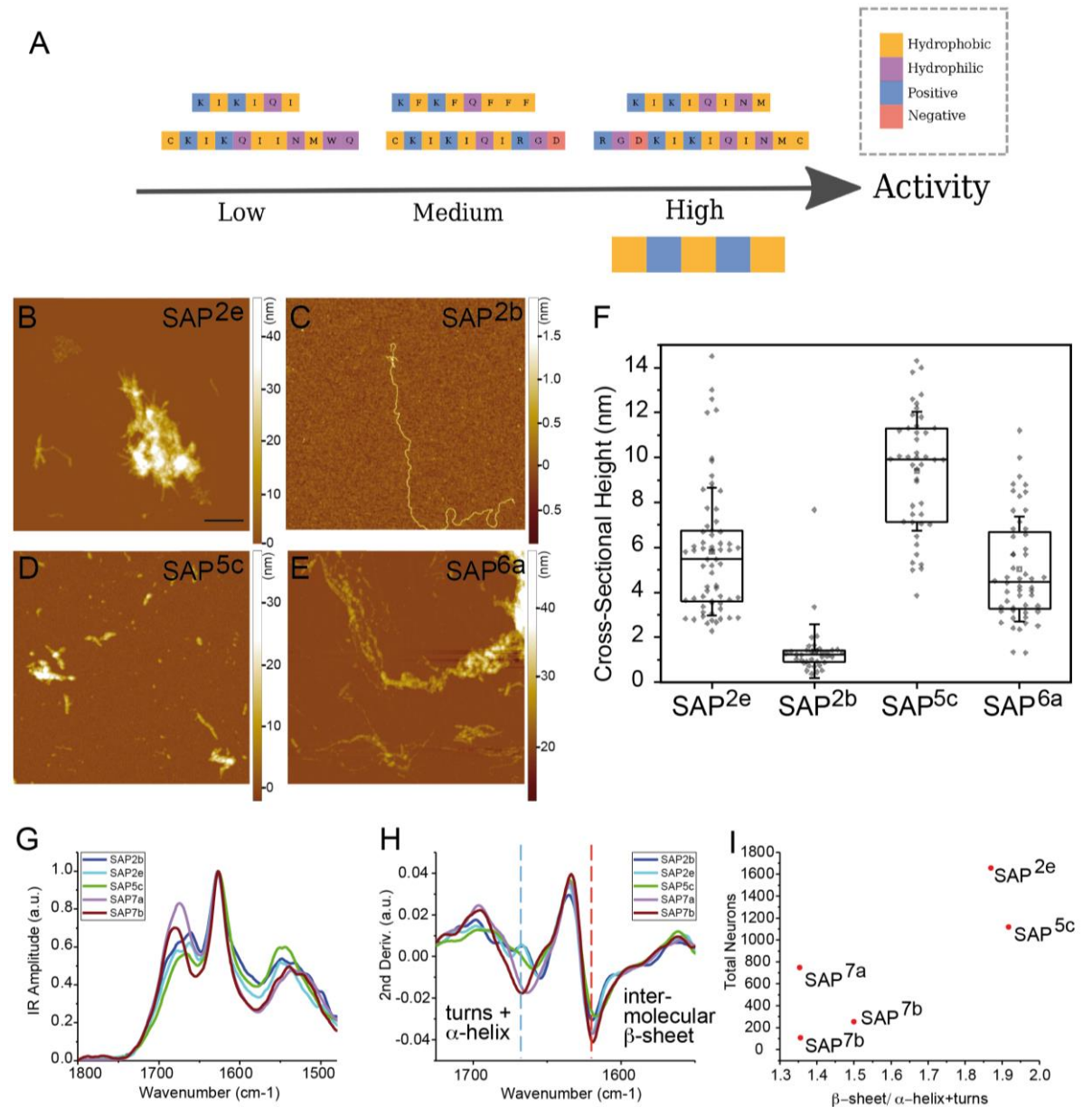

Figure 3. Rational analysis of SAP and PNF features to elucidate the important factors for neural activity
A) The structural motif of "active" SAP sequences essential for high neuronal activity was identified using a statistical analysis and is shown in the figure in coarse-grained representation. B-F) AFM analysis of PNF morphologies. Examples of individual PNFs from different SAPs are depicted in B-E. Measurement of cross-sectional height of several PNFs (F). Scale-bars (B-E) = 500 nm. G-I) Analysis of PNF structure by FT-IR spectroscopy. (G) IR spectra of selected SAPs normalized to the amide I band. (H) 2nd derivative of IR spectra for

secondary structure analysis. (I) The total number of neurons correlates with the ratio of ß-sheets to α-helix and turns.

Table 1 gives an overview of the morphologies of all PNFs that were obtained by 2-D TEM micrographs as discussed above. It is known that β-sheet structures within the PNF have an important impact on their persistence lengths and stiffness. Therefore, the β-sheet structures in PNFs were first characterized by the blue-shifted emission of Proteostat® (Figure S10). Most SAPs, which formed PNFs or aggregates in TEM investigations, also showed a fluorescence enhancement in the presence of Proteostat®. However, some PNFs did not incorporate the dye (e.g. SAP[2d], SAP[4d]). SAP[3b] revealed a significant fluorescent enhancement, but no PNFs in TEM investigations (Figure S3 and S10). The 3-D morphology of two pairs of SAPs with similar sequences was then analyzed with sub-nanometer resolution by phase controlled atomic force microscopy (AFM)[19]. We performed a single PNF statistical analysis by AFM to determine the cross-sectional fiber height [20] (Figure 3B-F, Figure S11). The fibrous morphology found in TEM images was confirmed (Figure 3B-F). Interestingly, the cross-sectional height of PNFs formed from SAP[2b] (KFKFQF) and SAP[2e] (CKFKFQF) differed significantly. This was an unexpected observation as both SAPs had a similar sequence with a terminal cysteine as the only difference. SAP[2b] (1.4 ± 0.4 nm) without the cysteine showed a significantly lower cross-sectional height than SAP[2e] (5.8 ± 0.5 nm; Figure 1L). The same trend was found for SAP[5c] compared to SAP[6a] (9.4 ± 0.5 nm vs. 5 ± 0.5 nm; Figure 3F).

To determine secondary structural elements in a more quantitative fashion, [22] FT-IR spectroscopy of lyophilized PNFs was performed and signals in the amide I band region in the range of 1625-1635 cm^{-1} (Table 1, Figure S12) corresponding to intermolecular β-sheet conformation as well as signals between 1650 – 1680 cm^{-1}, corresponding to α-helices and turns were analyzed. Obviously, the β-sheet content

within the PNFs varied and we could clearly observe from the FT-IR spectra an increase of the ß-sheet content for highly active SAP[2e] and SAP[5c].

By combining the structural and physico-chemical information of the PNFs with the data on neuronal activity obtained from the automated screen, critical parameters that define the biological activity of the SAPs were identified (summarized in Table S4). First, (1) PNF morphology and high conversion rates were essential for bioactivity. SAP[1d], for example, showed a low conversion rate of appr. 5%, indicating its poor ability to form assemblies, consequently preventing the formation of PNFs that could interact with cells. (2) Positive surface charges appear essential for interactions with neurons. SAP[8a] and SAP[6a] form fibers with negative zeta potentials that did not show high neuronal activity. (3) A significant intermolecular β-sheet signal in FT-IR, such as for SAP[2e] and SAP[5c] (Figure 3G-I) was clearly correlated with increased cross-sectional height and high neuronal activity. Positively charged PNFs that did not exhibit strong β-sheet signals only revealed moderate to low neuronal activity (see for example SAP[2b], SAP[7a], and SAP[7b]). Interestingly, the intermolecular β-sheet coincides with a higher fiber diameter, as measured by AFM, indicating that the thicker fibers likely provide higher stiffness and persistence length compared to their non-mature counterparts (compare SAP[2e] and SAP[2b]). However, the change in the fiber thickness may also change the surface of the fibers, which could also contribute to their biological performance.

2.4 SAP derived nanofibers enhanced neuronal adhesion in the stripe assay and Schwann cell adhesion and growth

In order to further test SAPs as substrates for neuronal growth, we employed the so-called stripe assay ([27]; Figure S13). Here, *bona fide* growth promoting substrates are arranged in alternating stripes interspersed by control lanes. We prepared alternating

stripes consisting of RITC (Rhodamine B isothiocyanate)-conjugated SAP[5c] and glass (Figure S13A). Indeed, DRG neurites preferred to grow on stripes containing SAP[5c] (Figure S13A). In fact, some neurites were crossing a SAP[5c]-free stripe to connect to the next available SAP[5c] stripe. In addition to neurites that preferentially adhered to SAP[5c]-positive stripes, also neuronal cell bodies (arrows Figure S13A) and non-neuronal DAPI positive cells showed a strong tendency to grow on SAP[5c] stripes (blue in Figure S13A).

As control, we used assays with both stripes containing SAP[5c] (Figure S13B, D). Here, we observed a randomized outgrowth of DRG neurites (Figure S13B, D). The stripe assay results show that DRGs neurons prefer to grow on SAP substrates with high bioactivity.

So far, the impact of SAPs was primarily tested on neurons (Figures 2 and S13). However, Schwann cells, the PNS myelinating cells, also influence outcome of axon regeneration [28]. Thus, the impact of SAPs on Schwann cell function was analyzed since SAPs may exert a positive influence on both neurons and Schwann cells, leading to a synergistic effect in axon regeneration (Figure S14).

Primary S100-positive Schwann cells derived from DRGs interacted with RITC-conjugated SAP[2e] positive plaques (Figure S14A) similarly to neurons (see Figure 1). All three selected SAPs, SAP[2e], SAP[1e] and SAP[5c] elevated Schwann cell adhesion (Figure S14G) and size (Figure S14H) compared to uncoated glass. Notably, all three SAPs provided a growth scaffold for this glial cell type, which was about as potent as laminin (Figure S14G, H). Thus, SAPs increased adhesion and growth in several cell types including neurons and glia cells.

2.5 SAPs stick in the lesion center of lesioned peripheral nerves

In previous experiments, selected SAPs stimulated outgrowth of primary neurons. In the next step, we assessed the potential of these SAPs to potentiate axon regeneration *in vivo*. We employed a mouse PNS lesion model where the facial nerve branches that connect motorneurons in the brainstem with several facial muscles responsible for triggering e.g. whisker movement are surgically injured (Figure 4A; [29]).

In the first set of experiments, we tested the time-window of SAPs to remain in the lesion site and determined the precise SAP localization with regard to the severed
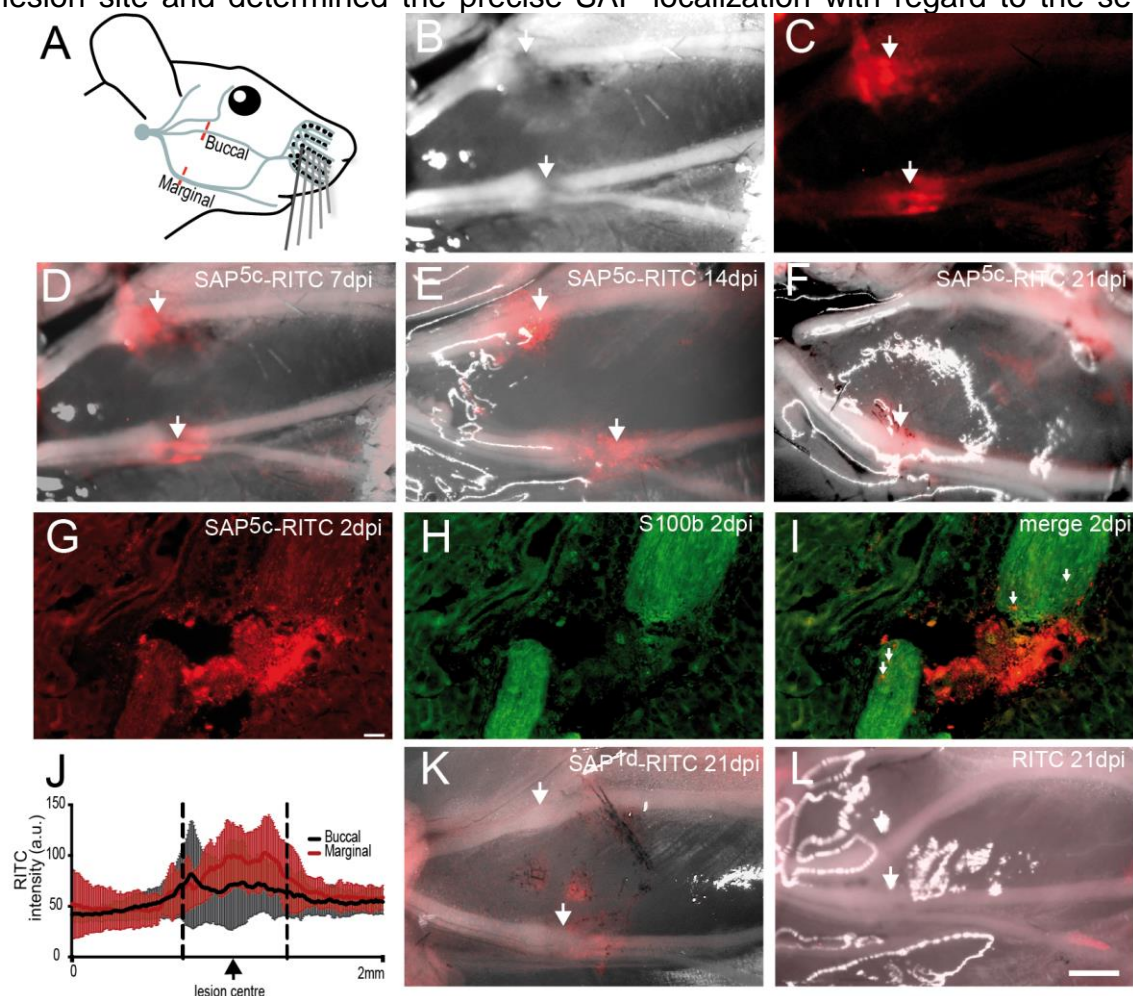

Figure 4. SAPs stick to injured nerves for up to three weeks
(A) Overview of the mouse facial nerve (blue) with lesion sites (red lines) at the buccal and marginal branch. (B-F) SAP^{5c}-RITC was injected into the lesion site and nerve preparations were analyzed at one (B-D), two (E) or three (F) weeks after injury. (B-D) shows light microscopical picture of the nerve (B), the same nerve with RITC fluorescence alone (C) and the composite picture (D). Arrows indicate the lesion and SAP injection site. (G-I) Section through the nerve stumps at 2 dpi stained for SAP^{5c}-RITC (G) and S100b to label Schwann cells in the nerve (H) and the merged picture (I). SAP^{5c}-RITC was found between the nerve stumps but also inside the nerve (arrows in I). (J) Quantification of SAP^{5c}-RITC intensity at the buccal and marginal branch in the lesion center and surrounding nerve. Strongest signals were observed in the lesion center. (K) SAP^{1d}-RITC, a SAP only weakly producing nanofibers, resulted in faint signals around the two lesion sites (arrows). (L) RITC not conjugated to a SAP did not adhere to the facial nerve. Scale-bars (B-F; K, L) = 1 mm; (G-I) = 50 µm

nerve stumps. This was important, since rapid diffusion away from the injury site and random localization of any biomaterial would not support stimulation of axon regeneration. Therefore, RITC-conjugated SAP[5c] (SAP[5c]-RITC) was injected into the lesioned buccal and marginal nerve branch (Figure 4A). Subsequently, whole amount preparations of the nerve and underlying muscle were analyzed at seven (Figure 4B-D), 14 (Figure 4E) and 21 (Figure 4F) days after injury. We observed perseverance of fluorescence signal originating from SAP[5c]-RITC located precisely at the injury site at several timepoints along the entire three-week period after injury (Figure 4B-F). The ability of the SAPs to remain at the injection site *in vivo* is further supported by SAP[5c]-fibers persisting in the presence of proteinase K (Figure S15). We further inspected PNF localization on histological sections through the two nerve stumps (Figure 4G-I). PNFs were found exactly in the gap between two nerve stumps and also in the facial nerve (arrows Figure 4I). Quantification of the staining intensity of SAP[5c]-RITC confirmed enrichment of the PNFs in the lesion center (Figure 4J). We wondered whether the highly adhesive properties of SAP[5c] were due to their potential to form fibrils. As a control experiment, we injected RITC alone and almost no signal was detectable (Figure 4L) arguing again for a role of the SAP part in mediating tissue interaction. SAP[1d]-RITC with a weak tendency to form PNFs (Figure 4K; see Figure S3) was added and resulted in only weak signals (Figure 4K) indicating that PNF formation contributed to high tissue adhesiveness of SAPs. Most likely, the positive charge of the PNFs was responsible for their stickiness. Also, binding of negatively charged HSA to SAP[5c] was demonstrated, further supporting their direct interaction with cellular structures such as cellular protrusions. In summary, we succeeded in administering the SAPs to a precise localization and – importantly – the SAPs persisted at the injection site for prolonged periods of time, indicating good stability during axon regeneration.

2.6 The SAP[5c] enhances peripheral nerve regeneration

Since SAPs used in this study showed strong adherence to nerve tissue (Figure 4), next we assessed their potential to augment facial nerve regeneration (Figures 5 and 6). For this, we again performed unilateral lesion to the mouse facial nerve and injected SAP[5c]-RITC or - as control – PBS in the lesion site (Figure 5). We also used SAP[1d], a SAP previously shown to have no neurite growth propagating potential and a weak tendency to form nanofibers (Figures 2, 4). Here, axon regeneration was similar to the negative control PBS (data not shown). After injection, the extent of nerve regeneration was analyzed by several histological parameters at 7, 14, or 21 days post injury (dpi). First, we analyzed retrograde transport of a fluorescent tracer (FG) injected into the whisker pads (Figure 5A-D; Q). Upon successful axonal regeneration, FG is retrogradely transported from the whisker pad via the re-connected nerves to the facial motorneurons [23, 30]. FG-positive neurons were counted and normalized to numbers obtained on the intact facial nucleus presenting maximal FG transport along axons. At 7 days post injury, approximately 30% of all MNs were FG-positive indicative of successful regeneration, however without any difference between experimental groups (Figure 5Q). One week later, this percentage doubled and SAP[5c]-injected animals already showed a tendency towards higher numbers of FG-positive MNs (Figure 5Q). After three weeks of injury we obtained a statistically significant increase in facial nerve regeneration in the SAP[5c] group compared to PBS treated animals (Figure 5C, D; Q). Now, SAP[5c] treated animals showed approximately 30-40% more FG-positive MNs than animals treated with PBS (Figure 5Q). The total MN number staining positive for Nissl was comparable between conditions (data not shown) thus indicating that SAP[5c] effects are not due to altered neuron death or survival.
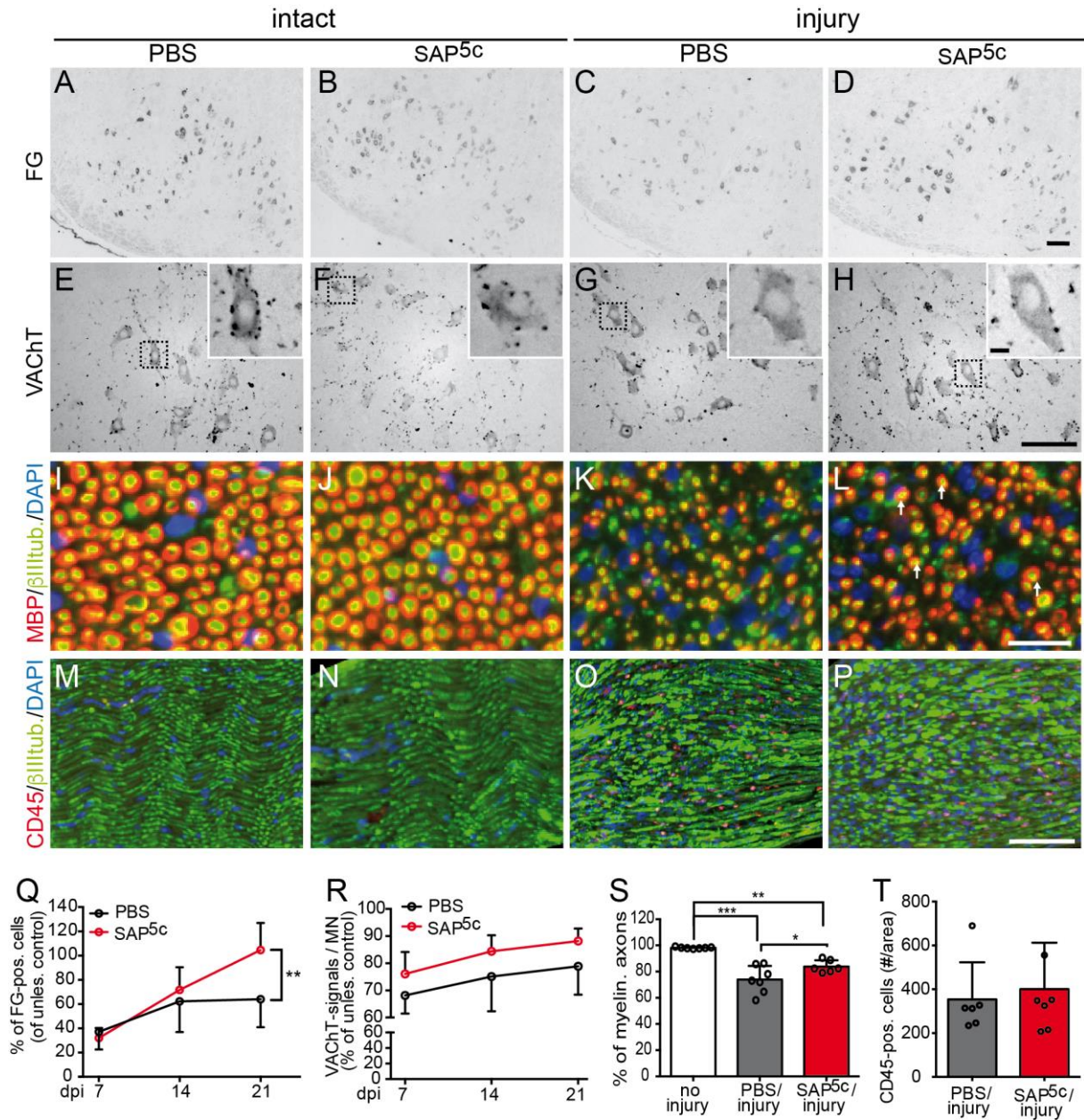
Figure 5. SAP5c improves several histological parameters of facial nerve regeneration
(A-D) Number of tracer (FG) positive neurons are depicted at 21 dpi. In the intact facial nucleus, numbers of FG-positive MNs are identical in PBS- (A) and SAP5c- (B) injected animals. After injury more FG-positive MNs are present in SAP5c- (D) compared to PBS- (C) treated animals. (B-H) The number of VAChT positive axonal sprouts was higher upon SAP5c injection (H) in comparison to PBS (G) at 21 dpi. Inserts show higher magnification of MNs marked with dashed lines. (I-L) Axons and myelin of facial nerves were stained with βIII tubulin and MBP, respectively. At 21 dpi, the number of myelinated axons was higher in SAP5c- (arrows in L) compared to PBS- (K) treated animals. (M-P) Peripheral CD45-positive immune cells were present in the facial nerve at 7 dpi at a comparable extent in PBS- (O) and SAP5c- (P) injected animals. Without injury, no CD45-positive cells are present (M, N). (Q) Quantification of FG-positive MNs at three time-points post injury. Data are normalized to the non-injured condition (set to 100%). (R) Quantification of VAChT signals/MN at three time-points post injury. Data are normalized to the non-injured condition (set to 100%). (S) Quantification of myelinated axons after injury. Intact nerves were set to 100%. Each circle reflects one animal.
(T) Quantification of CD45-positive cells in the facial nerve. No differences between groups were observed. Each circle reflects one animal.

Scale-bars (A-D; E-H; M-P) = 100 µm; (E-H inserts) = 10 µm; (I-L) = 20 µm

Next, we tested the abundance of vesicular acetylcholine transporter (VAChT; Figure 5E-H; R) whose abundance is down-regulated during motorneuron degeneration and increasing once axons start to regenerate [31]. We analyzed VAChT abundance at all three time-points after injury and normalized numbers to intact facial nuclei of PBS (Figure 5E) or SAP5c-treated (Figure 5F) animals. In line with previous reports [31], VAChT was distributed mainly at the periphery of cell bodies (Figure 5E-H). At 7 dpi VAChT numbers were reduced by approximately 30-35% compared to intact MNs and numbers gradually increased up to 90% at 21 dpi (Figure 5R). Importantly, at all three time-points SAP5c-treated animals (Figure 5H) showed on average 10% more VAChT positive sprouts compared to the PBS-injected animals (Figure 5G; R).

In the nerve injury, so-called Wallerian degeneration triggers nerve degeneration and removal of myelin resulting in un-myelinated axons [32]. Indeed, numbers of myelinated axons decreased 21 dpi (Figure 5K, L) by about 30% compared to intact nerves in either experimental group (Figure 5I, J). Facial nerves injected with SAP5c-RITC (arrows Figure 5L) had 10% more myelinated axons compared to nerves receiving PBS (Figure 5K) suggesting that SAP5c can enhance re-formation of myelinated axons (Figure 5S).

Finally, we analyzed infiltration of peripheral CD45-positive immune cells into the facial nerves to control for a potential augmented immune response elicited by the SAPs (Figure 5M-P; T). We observed entry of immune cell specifically in the injured (Figure 5O, P) and not control (Figure 5M, N) nerve at 7 dpi. However, quantification revealed no additional immune cell infiltration by the SAP injection (Figure 5T). Thus, as also observed in previous reports [7c], SAPs do not appear to trigger an immune response in the host tissue. In summary, several histological parameters of PNS regeneration showed enhanced facial nerve regeneration in animals injected with SAP5c.

2.7 SAP[5c] enhanced physiological recovery of whisker movement after injury

Histological inspection already suggested enhanced motorneuron recovery after injury by SAP injection (Figure 5). However, this does not automatically result in the recovery of physiological function of injured nerves. In order to analyze whether nerve regeneration also enhanced function of the neuromuscular unit controlling whisker movement, we performed timelapse-videomicroscopy as reported by others [33] and us [34] before (Figure 6). Here, individual vibrissae of both sides of the animals were recorded before and at several timepoints after injury (Figure 6A). Typically, whisker movement of both sides is synchronized as shown by our quantification (Figure 6D). One day after injury, whisker movement is impaired on the injured side (see video trace in Figure 6E) and vibrissae engage a stiff position pointing towards one direction (arrows Figure 6B). At 18 dpi whisker movement is partially restored (Figure 6C) and the injured whiskers (black line in Figure 6F) start to rotate again.

When comparing PBS- and SAP[5c]-injected animals (N = 7 each) we observed in both groups an identical drop in whisker movement at 1 dpi for two parameters, sum of all angles rotated (Figure 6G) and maximal amplitude (Figure 6H). Within the next 18 days, whisker movement increased in both groups. However, we noted that recovery in SAP[5c]-treated compared to PBS-treated animals was enhanced (Figure 6G, H). This was evident with the angular range (Figure 6H) and even more pronounced when inspecting the angular sum (Figure 6G) at several time-points post injury showing that SAP[5c] enhanced regeneration in comparison to the PBS treated animals. However, statistical significance was not reached between PBS and SAP
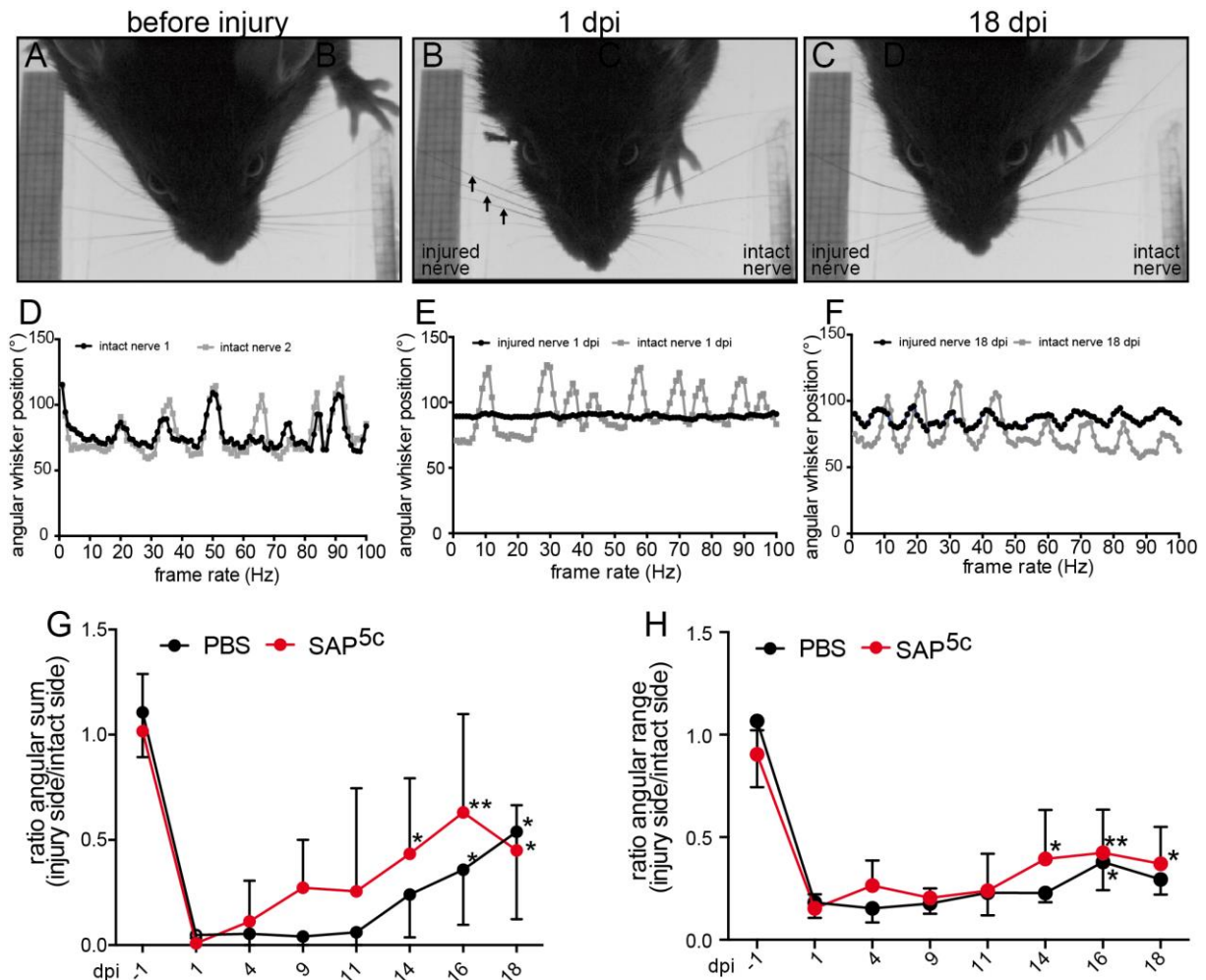
Figure 6. Recovery of whisker movement is enhanced by SAP5c-injection

(A-C) Representative pictures of whisker position before injury (A), one (B) and 18 (C) dpi. One day after injury, vibrissae of the injured whisker pad (arrows) cannot move and point all towards the same position. (D-F) Representative whisker traces from a 100 Hz sequence. Without injury, vibrissae from both sides rotate synchronously (D). At 1 dpi, whiskers do not move at the injured side (black line E) whereas movement is possible on the contralateral side (grey line in E). At 18 dpi, whisker movement at the injured side recovers to some extent (black line in F). (G) All movements with angles ≥ 10° were summed up in a 100 Hz sequence. A ratio between injured to un-injured side was calculated and plotted along several time-points of measurement. Whisker movement in SAP[5c]-injected animals (red line) recovered quicker than in PBS-treated (black line) animals. (H) The maximal amplitude of whisker movement is depicted. SAP5c-treated animals had in general higher amplitude than the PBS control group.

treated groups and would require more animals to be included. As control, we again employed SAP[1d], a SAP with no obvious biological activity (Figure 2). PBS- and SAP[1d]-injected animals were indistinguishable with regard to whisker recovery (data not

shown). We also tested SAP[2e] as a second active SAP that also enhanced whisker movement compared to PBS treated animals although weaker compared to SAP[5c] (data not shown). These first results are very promising and show that SAPs have the potential to not only enhance histological parameters of nerve regeneration (Figure 5) but also functional recovery of motor functions (Figure 6). We believe that additional experiments e.g. for dose finding will be required to further boost the *in vivo* effectiveness.

3 Discussion

Structural features of SAPs for the modulation of cellular adhesion and growth

We have shown that SAPs are a promising and versatile biomaterial in neuronal regeneration. In our studies, several unmodified but also RGD-functionalized SAPs stimulated adhesion and growth of nerve cells (Figure 2; Figure S4). Fibril formation was a prerequisite for cell growth stimulation as SAP[1d] with moderate fibril formation and conversion rate only weakly promoted neurite growth (Figure 2). Only when fibril formation was induced in SAP[1d] through Fmoc–functionalization (now called SAP[1e]) strong neurite growth potential was observed (Figure 2). A data mining approach allowed us to identify a general amino acid pattern that could propose high-activity peptide sequences (Figure 3) based on alternating hydrophobic and positively charged amino acids ($H^0P^+H^0P^+H^0$). The positive charges are essential as they provide "stickiness", which seems essential for direct *in vivo* application.

Interestingly, we observed a strong correlation between the cross-sectional height of the fibers and their activity (Figure 1; Figure S11). Materials such as SAP[2e] and SAP[5c] formed fibers of significantly larger diameter and revealed much higher activity on neuronal growth than their analogues without a terminal cysteine group (SAP[2b] and SAP[6a]). We attributed the change in cross-sectional height to a difference in the

maturity of amyloid fibers and to a different surface structure consequently leading to a change of activity. In addition, the nanofiber diameter is correlated to an increased persistence length of the fibrils that is likely to be positively correlated with higher stiffness of the fibrils. It is known that substrate stiffness affects neuronal growth [38] and increased substrate stiffness enhances DRG growth in particular [39], which is in agreement with our data (Figure 2).

We observed that the unmodified SAP backbone SAP[1e], SAP[4e], SAP[2c] and e.g. SAP[4b] already provided a good growth substrate (Figures 2; Figures S4 and S5). This adhesiveness might be mediated by electrostatic forces of negatively charged cell membranes interacting with positively charged nanofibers. This observation is further supported by the lack of cell adhesion on SAPs with a net negative charge (Figure S1). Additional functional groups such as the RGD sequence in SAP[5c], SAP[5b] and SAP[5d] further augmented the potential of SAPs to enhance neuronal growth (Figure 2). In fact, SAP[5c]-derived nanofibrils gave best results in our *in vivo* PNS regeneration model (Figures 5 and 6). In addition to testing the linear RGD epitope, we also analyzed cyclic RGD, which did not further increase nerve fiber growth (data not shown). Interestingly, only N-terminal but not C-terminal RGD (e.g. SAP[6a], SAP[6b]) SAP modifications provided a boost in activity (Figures 1 and 2). This points towards a potential sterical hindrance of the RGD epitope at the C-terminus preventing its surface exposure and possibly interaction its cognate cellular integrin receptor.

Direct SAP nanofibril injection as tool in tissue regeneration

The SAP activity was not limited to individual cell types but they exhibited a wide range of bioactivities including stimulation of cell adhesion and growth of glial and neuronal cells derived from both the PNS and CNS (Figures 2; Figure S4, S5, and S13). Considering previous reports on SAP-mediated activity on muscle cells [35], stem cells

[36] and e.g. bone cells [37], these results suggest that SAPs represent a versatile extracellular-matrix mimicking biomaterial providing adhesion and growth support to many different cell types in the CNS and PNS.

In this study we used a novel approach to deliver SAP-derived PNFs to injured tissue in living animals. PNFs in solution were directly applied to the injury site without any additional incorporation into hydrogels or artificial nerve conduits (Figures 4-6). This was only possible since the newly discovered and optimized SAPs used in this study provided high adhesive properties to tissues (Figure 4). Importantly, this "stickiness" was not temporary but lasted for at least three weeks after injury (Figure 4). Such a time window is sufficient to induce enhanced regenerative cell processes during axonal regeneration as investigated in this mouse study (Figures 5 and 6) but also in other injured organs. For instance, PNFs could be used to fill cavities formed during bone fracture, CNS spinal cord lesions or traumatic brain injury. In support for the latter we demonstrated already that selected SAPs identified in this study enhance outgrowth of CNS neuron types (Figure S5).

In all parameters of axonal regeneration the RGD-containing SAP^{5c} was superior to PBS control or other SAPs thereby highlighting the specificity of SAP^{5c} results obtained (Figures 5 and 6). It is rather challenging to directly compare our data with previously reported PNF approaches since often, different species (rat vs. mouse), model systems (e.g. facial vs. sciatic nerve), application routes (hydrogels, tubes conduits etc.), time-points after injury (3-8 weeks) were used. For instance, in mice, the application of nerve autografts[15] as positive control could not be used since an autograft of the mouse facial nerve is far too small to suture it to an injured nerve stump. Therefore, the regeneration outcome was compared to PBS injection in the lesion site as negative control. In addition, depending on the disease model, different

regeneration parameters (histological, physiological, molecular) were employed, which also limits a direct one-to-one comparison.

We observed on the histological level, that SAPs used in our study elevated regeneration between 10-40% depending on histological read-out (Figure 4Q-S). This is in concordance with previously achieved results, for instance the effect of the RADA 16 nanofibers that elevated numbers of axons reinnervating target muscles by 10-20% [16a, 16b]. For functional regeneration, e.g. recovery of limb movement or whisking in sciatic or facial nerve injury, respectively, data are in general more heterogenous which is often due to variability between injured animals. In our study, SAP[5c] was able to enhance functional recovery of whisker movement to approximately 40-50% or pre-injury values at 14 days post injury (Figure 6). Similar to us, in the only other facial nerve injury study available using VVVAAAEEE nanofibers, the authors observed that the maximum nerve compound action potentials reached 40% of pre-injury levels. However here, much longer time-points were required for regeneration (i.e. 8 weeks). In sciatic nerve injury, VVAAEE [16c] or the RADA 16 derived nanofibers [16a] enhanced functional recovery of limb motor function by 10-20%. Thus, with all the caution that should be taken into consideration when comparing regeneration data between different model systems and experimental set-ups, data obtained on nanofibers in this study reached levels at least comparable to previous reports. We would like to stress that the SAP material designed and used in this study achieved all effects without the need to additionally use tubes, hydrogels or other conduits that were required in previous studies, which clearly simplifies their applications.

Conclusions

From a library of 27 short SAPs forming nanofibers with an internal β-sheet structure, we identified peptide sequences that stimulated the growth and adhesion of primary

mouse PNS and CNS neural cells. Highly active peptides have (1) a strong propensity to form fibers, (2) consist of an alternating pattern of hydrophobic and positively charged amino acids and positive net charge, (3) showed higher β-sheet contents and (4) a larger cross-sectional diameter in single fiber AFM analysis. After direct injection of the sticky SAPs into the site of injury in an *in vivo* PNS lesion model of the facial nerve, the PNFs remained at the lesion site for several weeks. Furthermore, the SAPs promoted the regeneration of the facial nerve, leading to improved functional recovery of the whisker movement. These results indicate the potential of optimized SAP nanofibrils as a promising, cost-effective, and labor-saving material for tissue engineering also applicable to other tissues including brain, bones, heart or muscle.

In preliminary results we noted that SAPs can interact with proteins when mixed in solution (Figure S16). Thus, we envision that the SAP-based PNFs could serve as versatile platform for further functionalization by binding other proteins upon mixing for attaching e.g. active growth factor domains of e.g. NGF or GDNF (glial derived neurotrophic factor; [40]), which offers great potential to further boost PNS nerve fiber growth.

Author Disclosure Statement

The authors declare no competing interests.

References

[1]   a) K. M. Koss, L. D. Unsworth, *Materials* 2018, 11; b) M. D. Sarker, S. Naghieh, A. D. McInnes, D. J. Schreyer, X. Chen, *Progress in neurobiology* 2018, DOI: 10.1016/j.pneurobio.2018.07.002.

[2]   A. C. Pinho, A. C. Fonseca, A. C. Serra, J. D. Santos, J. F. Coelho, *Adv Healthc Mater* 2016, 5, 2732.

[3]   a) B. Jiang, P. Zhang, B. Jiang, *Artificial cells, blood substitutes, and immobilization biotechnology* 2010, 38, 1; b) D. P. Kuffler, *Progress in neurobiology* 2014, 116, 1.

[4]   N. D. Fagoe, J. van Heest, J. Verhaagen, *Neuromolecular medicine* 2014, 16, 799.

[5]   a) Y. Loo, M. Goktas, A. B. Tekinay, M. O. Guler, C. A. Hauser, A. Mitraki, *Adv Healthc Mater* 2015, 4, 2557; b) R. Pugliese, F. Gelain, *Trends in biotechnology* 2017, 35, 145; c) C. M. Rubert Perez, N. Stephanopoulos, S. Sur, S. S. Lee, C. Newcomb, S. I. Stupp, *Annals of biomedical engineering* 2015, 43, 501.

[6]   J. B. Matson, S. I. Stupp, *Chemical communications* 2012, 48, 26.

[7]   a) S. S. Negah, A. Khooei, F. Samini, A. Gorji, *Cell and tissue research* 2017, DOI: 10.1007/s00441-017-2739-0; b) V. M. Tysseling, V. Sahni, E. T. Pashuck, D. Birch, A. Hebert, C. Czeisler, S. I. Stupp, J. A. Kessler, *Journal of neuroscience research* 2010, 88, 3161; c) V. M. Tysseling-Mattiace, V. Sahni, K. L. Niece, D. Birch, C. Czeisler, M. G. Fehlings, S. I. Stupp, J. A. Kessler, *The Journal of neuroscience : the official journal of the Society for Neuroscience* 2008, 28, 3814.

[8]   S. Sieste, Mack, T., Synatschke, C.V., Schilling, C., Meyer zu Reckendorf, C., Pendi, L., Harvey, S., Ruggeri, F.S., Knowles, T.P.J., Meier, C., Ng, D.Y.W., Weil, T., and Knoll, B. , *Advanced Healthcare Materials* 2018, accepted.

[9]   B. Mammadov, M. Sever, M. Gecer, F. Zor, S. Ozturk, H. Akgun, U. H. Ulas, Z. Orhan, M. O. Guler, A. B. Tekinay, *RSC advances* 2016, 6, 110535.

[10]   a) A. L. Rodriguez, K. F. Bruggeman, Y. Wang, T. Y. Wang, R. J. Williams, C. L. Parish, D. R. Nisbet, *Journal of tissue engineering and regenerative medicine* 2018, 12, e1571; b) W. Shi, C. J. Huang, X. D. Xu, G. H. Jin, R. Q. Huang, J. F. Huang, Y. N. Chen, S. Q. Ju, Y. Wang, Y. W. Shi, J. B. Qin, Y. Q. Zhang, Q. Q. Liu, X. B. Wang, X. H. Zhang, J. Chen, *Acta biomaterialia* 2016, 45, 247.

[11]   C. Lu, Y. Wang, S. Yang, C. Wang, X. Sun, J. Lu, H. Yin., W. Jiang, H. Meng, F. Rao, X. Wang, J. Peng, *ACS Biomaterials* 2018, 4, pp 2994.

[12]   a) Z. Huang, C. J. Newcomb, Y. Lei, Y. Zhou, P. Bornstein, B. A. Amendt, S. I. Stupp, M. L. Snead, *Biomaterials* 2015, 61, 216; b) S. Sur, F. Tantakitti, J. B. Matson, S. I. Stupp, *Biomaterials science* 2015, 3, 520.

[13] a) E. J. Berns, S. Sur, L. Pan, J. E. Goldberger, S. Suresh, S. Zhang, J. A. Kessler, S. I. Stupp, *Biomaterials* 2014, 35, 185; b) T. C. Holmes, S. de Lacalle, X. Su, G. Liu, A. Rich, S. Zhang, *Proceedings of the National Academy of Sciences of the United States of America* 2000, 97, 6728; c) Z. Zou, Q. Zheng, Y. Wu, X. Guo, S. Yang, J. Li, H. Pan, *Journal of biomedical materials research. Part A* 2010, 95, 1125.

[14] a) F. Gelain, S. Panseri, S. Antonini, C. Cunha, M. Donega, J. Lowery, F. Taraballi, G. Cerri, M. Montagna, F. Baldissera, A. Vescovi, *ACS nano* 2011, 5, 227; b) Y. Liu, H. Ye, K. Satkunendrarajah, G. S. Yao, Y. Bayon, M. G. Fehlings, *Acta biomaterialia* 2013, 9, 8075.

[15] J. J. Greene, M. T. McClendon, N. Stephanopoulos, Z. Alvarez, S. I. Stupp, C. P. Richter, *Journal of tissue engineering and regenerative medicine* 2018, 12, 1389.

[16] a) X. Wu, L. He, W. Li, H. Li, W. M. Wong, S. Ramakrishna, W. Wu, *Regenerative biomaterials* 2017, 4, 21; b) X. Wang, M. Pan, J. Wen, Y. Tang, A. D. Hamilton, Y. Li, C. Qian, Z. Liu, W. Wu, J. Guo, *Neural regeneration research* 2014, 9, 2132; c) A. Li, A. Hokugo, A. Yalom, E. J. Berns, N. Stephanopoulos, M. T. McClendon, L. A. Segovia, I. Spigelman, S. I. Stupp, R. Jarrahy, *Biomaterials* 2014, 35, 8780.

[17] a) M. Yolamanova, C. Meier, A. K. Shaytan, V. Vas, C. W. Bertoncini, F. Arnold, O. Zirafi, S. M. Usmani, J. A. Muller, D. Sauter, C. Goffinet, D. Palesch, P. Walther, N. R. Roan, H. Geiger, O. Lunov, T. Simmet, J. Bohne, H. Schrezenmeier, K. Schwarz, L. Standker, W. G. Forssmann, X. Salvatella, P. G. Khalatur, A. R. Khokhlov, T. P. Knowles, T. Weil, F. Kirchhoff, J. Munch, *Nature nanotechnology* 2013, 8, 130; b) C. Meier, T. Weil, F. Kirchhoff, J. Munch, *Wiley interdisciplinary reviews. Nanomedicine and nanobiotechnology* 2014, 6, 438.

[18] a) A. Lampel, R. V. Ulijn, T. Tuttle, *Chemical Society reviews* 2018, 47, 3737; b) S. Das, K. Zhou, D. HGhosh, N. N. Jha, P. K. Singh, R. S. Jacob, C. C. Bernard, D. I. Finkelstein, J. S. Forsythe, S. K. Maji, *NPG Asia Materials* 2016, 8; c) E. V. Alakpa, V. Jayawarna, K. E. V. Burgess, C. C. West, B. Peault, R. V. Ulijn, M. J. Dalby, *Scientific reports* 2017, 7, 6895.

[19] F. S. Ruggeri, S. Vieweg, U. Cendrowska, G. Longo, A. Chiki, H. A. Lashuel, G. Dietler, *Scientific reports* 2016, 6, 31155.

[20] F. S. Ruggeri, F. Benedetti, T. P. J. Knowles, H. A. Lashuel, S. Sekatskii, G. Dietler, *Proceedings of the National Academy of Sciences of the United States of America* 2018, 115, 7230.

[21] J. Gac anin, J. Hedrich, S. Sieste, G. Glasser, I. Lieberwirth, C. Schilling, S. Fischer, H. Barth, B. Knoll, C. V. Synatschke, T. Weil, *Advanced materials* 2018, DOI: 10.1002/adma.201805044e1805044.

[22] D. M. Byler, H. Susi, *Biopolymers* 1986, 25, 469.

[23] M. Gey, R. Wanner, C. Schilling, M. T. Pedro, D. Sinske, B. Knoll, *Open biology* 2016, 6.

[24] C. Meier, S. Anastasiadou, B. Knoll, *PloS one* 2011, 6, e26089.

[25] R. S. Jacob, D. Ghosh, P. K. Singh, S. K. Basu, N. N. Jha, S. Das, P. K. Sukul, S. Patil, S. Sathaye, A. Kumar, A. Chowdhury, S. Malik, S. Sen, S. K. Maji, *Biomaterials* 2015, 54, 97.

[26] R. K. Das, R. V. Pappu, *Proceedings of the National Academy of Sciences of the United States of America* 2013, 110, 13392.

[27] B. Knoll, C. Weinl, A. Nordheim, F. Bonhoeffer, *Nature protocols* 2007, 2, 1216.

[28] K. R. Jessen, R. Mirsky, A. C. Lloyd, *Cold Spring Harbor perspectives in biology* 2015, 7, a020487.

[29] L. B. Moran, M. B. Graeber, *Brain research. Brain research reviews* 2004, 44, 154.

[30] a) S. Di Giovanni, C. D. Knights, M. Rao, A. Yakovlev, J. Beers, J. Catania, M. L. Avantaggiati, A. I. Faden, *The EMBO journal* 2006, 25, 4084; b) G. Raivich, M. Bohatschek, C. Da Costa, O. Iwata, M. Galiano, M. Hristova, A. S. Nateri, M. Makwana, L. Riera-Sans, D. P. Wolfer, H. P. Lipp, A. Aguzzi, E. F. Wagner, A. Behrens, *Neuron* 2004, 43, 57.

[31] a) T. Ichimiya, S. Yamamoto, Y. Honda, R. Kikuchi, S. Kohsaka, K. Nakajima, *Brain research* 2013, 1507, 35; b) M. Makwana, A. Werner, A. Acosta-Saltos, R. Gonitel, A. Pararajasingham, C. Ruff, P. Rumajogee, D. Cuthill, M. Galiano, M. Bohatschek, A. S. Wallace, P. N. Anderson, U. Mayer, A. Behrens, G. Raivich, *The Journal of comparative neurology* 2010, 518, 699.

[32] A. D. Gaudet, P. G. Popovich, M. S. Ramer, *Journal of neuroinflammation* 2011, 8, 110.

[33] a) M. Grosheva, O. Guntinas-Lichius, S. Arnhold, E. Skouras, S. Kuerten, M. Streppel, S. K. Angelova, K. Wewetzer, C. Radtke, S. A. Dunlop, D. N. Angelov, *Biol Chem* 2008, 389, 873; b) O. Guntinas-Lichius, G. Hundeshagen, T. Paling, M. Streppel, M. Grosheva, A. Irintchev, E. Skouras, A. Alvanou, S. K. Angelova, S. Kuerten, N. Sinis, S. A. Dunlop, D. N. Angelov, *Neurobiology of disease* 2007, 28, 101.

[34] R. Wanner, M. Gey, A. Abaei, D. Warnecke, L. de Roy, L. Durselen, V. Rasche, B. Knoll, *Neuromolecular medicine* 2017, 19, 357.

[35] D. A. Harrington, E. Y. Cheng, M. O. Guler, L. K. Lee, J. L. Donovan, R. C. Claussen, S. I. Stupp, *Journal of biomedical materials research. Part A* 2006, 78, 157.

[36] F. A. Somaa, T. Y. Wang, J. C. Niclis, K. F. Bruggeman, J. A. Kauhausen, H. Guo, S. McDougall, R. J. Williams, D. R. Nisbet, L. H. Thompson, C. L. Parish, *Cell reports* 2017, 20, 1964.

[37] L. Lu, N. Arizmendi, M. Kulka, L. D. Unsworth, *Adv Healthc Mater* 2017, 6.

[38] K. Franze, P. A. Janmey, J. Guck, *Annual review of biomedical engineering* 2013, 15, 227.

[39] D. Koch, W. J. Rosoff, J. Jiang, H. M. Geller, J. S. Urbach, *Biophysical journal* 2012, 102, 452.

[40] J. Nielsen, K. Gotfryd, S. Li, N. Kulahin, V. Soroka, K. K. Rasmussen, E. Bock, V. Berezin, *The Journal of neuroscience : the official journal of the Society for Neuroscience* 2009, 29, 11360.

Max Planck Institute for Polymer Research – Author's Manuscript